Electron-impact excitation of singly charged metal ions

L. Sharma,[1,2,3] A. Surzhykov,[1,2] R. Srivastava,[3] and S. Fritzsche[2,4]
[1]*Physikalisches Institut, Universität Heidelberg, Philosophenweg 12, D-69120 Heidelberg, Germany*
[2]*GSI Helmholtzzentrum für Schwerionenforschung GmbH, Planckstrasse 1, D-64291 Darmstadt, Germany*
[3]*Department of Physics, Indian Institute of Technology, Roorkee 247667, India*
[4]*Department of Physics, Post Office Box 3000, FI-90014 University of Oulu, Finland*
(Received 23 February 2011; published 6 June 2011)

Fully relativistic distorted-wave theory has been applied to study the electron-impact excitation of the $ns_{1/2}$-$np_{1/2}$ and $ns_{1/2}$-$np_{3/2}$ resonance transitions of singly charged metal ions with one valence electron, viz., Mg^+ ($n = 3$), Ca^+ ($n = 4$), Zn^+ ($n = 4$), Cd^+ ($n = 5$), and Ba^+ ($n = 6$). Calculations are performed in the range of incident electron energies up to 300 eV for differential and integrated cross sections as well as for the linear polarization of the photon emissions following the decay of excited $np_{3/2}$ states. Results are compared with the available experimental data and previous nonrelativistic theoretical calculations. Moreover, analytic fits to our integrated cross sections are provided for potential applications in modeling plasma sources and environments.

DOI: 10.1103/PhysRevA.83.062701 PACS number(s): 34.80.−i

I. INTRODUCTION

Electron-impact excitation cross sections of atoms and ions are in great demand due to their many practical applications in modeling of fusion plasmas, plasma processing of semiconductors, and analyzing planetary atmospheres. Apart from the behavior and energy dependence of the excitation cross sections, a detailed analysis of the polarization properties of the characteristic photons emitted in the decay of excited atomic states helps to understand the emission line spectra observed in high-temperature plasmas. For excitation of neutral atoms extensive theoretical and experimental investigations are reported up to now and their findings have been in good agreement. These theoretical work have employed various sophisticated methods, e.g., nonrelativistic and relativistic distorted wave (RDW) [1–3], converged close coupling (CCC) [4], and R matrix [5].

In contrast to neutral atoms, less attention has been paid to the electron excitation of singly and multiply charged ions. For such ions, a great requirement for cross-section data has been pointed out as not enough data are available owing to the difficulties in performing the experiments. To meet this requirement, several calculations have been reported but with an emphasis on highly charged ions [6,7]. Therefore, calculations are still needed for singly ionized metal ions which play an important role in understanding heating and radiation mechanisms in a wide range of high electron-temperature plasmas. For metal ions, the available calculations are based on simple nonrelativistic theories only. To analyze the quality of these data, improved relativistic calculations for the excitation cross sections are desirable and should be performed.

There are some experiments which have been performed to study excitation of metal ions. For instance, Dunn and his coworkers measured excitation cross sections and polarization fraction for Ca^+, Zn^+, and Ba^+ [8–10] using the crossed-charged-beams technique. Chutjian and co-workers [11,12] reported the first measurements on the excitation and angular distribution of the fine-structure unresolved $4s$-$4p$ transition in Zn^+ at 75 eV using energy-loss techniques. Later, these authors [13,14] also performed similar (relative) differential cross-section measurement for the electron-impact excitation of optically forbidden and resonance transitions (ns-np) in Mg^+, Zn^+, and Cd^+. With the electron-energy-loss merged beams technique, Smith *et al.* [15] reported excitation cross sections for fine-structure resonance transition $ns_{1/2}$-$np_{1/2}$ in Mg^+ and Zn^+ for a limited range of electron energies. However, these latter measurements were found to be not very reliable since the energy-loss technique has severe limitations in measuring the data in a forward direction. Therefore, in order to obtain the integrated cross sections Smith and co-workers had to extrapolate their data in the forward direction, giving rise to rather large uncertainties in the experimental values [16].

A number of nonrelativistic fine-structure unresolved calculations were reported for metal ions. Among the recent theoretical works, Kim [16] applied a scaling method to Coulomb-Born cross sections for excitations of singly charged helium, magnesium, and zinc ions. Zatsarinny and Bandurina [17] investigated the low-energy electron-impact excitation of the $4s$-$4p$ transition in Zn^+ using the R-matrix method. Kennedy *et al.* [18] performed calculations using a unitarized distorted-wave polarized-orbital (UDWPOII) approximation and various forms of the Coulomb-Born (CB) approximation. They compared their results with the three-state close-coupling (CC) calculations of Burke and Moores [19]. The shortcoming of the UDWPOII calculations was that the distortion potential was included only in the initial channel but was omitted from the final channel. Such calculations are now known not to be consistent. Mitroy *et al.* [20] also presented a detailed study of electron-impact excitation of the resonance transition of Ca^+ in the limited low-energy range using only three- and six-state CC approximations as well as unitarized CB and distorted-wave (DW) approximations. Pindzola *et al.* [21] calculated excitation cross sections for the $4s$-$4p$ transition in Zn^+ using a multiple LS-term CC approximation. Pangantiwar and Srivastava [22] applied nonrelativistic distorted-wave (NRDW) theory to calculate differential cross sections for resonance transitions in Mg^+, Zn^+, and Cd^+.

Despite the various experimental results and a number of nonrelativistic CB, DW, and few three- to five-state CC calculations for electron-impact excitation of singly charged metallic ions, there is a lack of reliable relativistic calculations

for these ions. Relativistic effects are important and must be included for those atoms where spin-orbit coupling is important. In this contribution, we present a systematic study of electron-impact excitation of singly charged metal ions using the RDW theory. In our previous work we have successfully applied the RDW method to electron-impact excitation of various multielectron neutral atoms including inert gases [1,2,23] and provided differential and angle integrated cross sections as well as polarization of photon emission [3,24,25]. The same RDW theory has been extended to the electron-ion excitation, and is applied in the present study for singly charged metal ions. In our RDW method, multiconfiguration Dirac-Fock wave functions in j-j coupling have been used to describe the bound states of the target ions. The relativistic continuum wave functions are calculated by solving Dirac equations in the field of frozen target-ion charge distribution. In our present calculation, we have taken into account the relativistic Breit interaction in addition to the (usual) projectile electron-target Coulomb interaction, anticipating its contribution might be important for ions. No Breit corrections were included in our earlier RDW calculations for neutral atoms [1,2,23–26]. Using the RDW theory, we present here calculations for differential and integrated cross sections for the resonance transitions $ns_{1/2}$-$np_{1/2}$ and $ns_{1/2}$-$np_{3/2}$ in Mg^+ ($n = 3$), Ca^+ ($n = 4$), Zn^+ ($n = 4$), Cd^+ ($n = 5$), and Ba^+ ($n = 6$) in the electron-energy range up to 300 eV. In addition to the cross sections, calculations are performed also on the polarization of the photon emission following the decay of the $np_{3/2}$ state back into the $ns_{1/2}$ ground state in these ions. Finally, we compare our results with the available experimental and other nonrelativistic theoretical data.

II. THEORY

A. Scattering amplitude

As usual, all the properties of the excitation process can be expressed in terms of the scattering (transition) amplitude. This scattering amplitude can be written within the first-order perturbation theory as (atomic units will be used throughout)

$$\begin{aligned} &f(J_a,M_a,\mu_a;\ J_b,M_b,\mu_b,\theta) \\ &= (2\pi)^2\sqrt{\frac{k_b}{k_a}}\langle\phi_b(\mathbf{1},\mathbf{2},\ldots,N)F_b^{\mathrm{DW}-} \\ &\quad\times(\mathbf{k}_b,N+1)\,|V_{\mathrm{in}}-V_d(N+1)| \\ &\quad\times\mathcal{A}\phi_a(\mathbf{1},\mathbf{2},\ldots,N)F_a^{\mathrm{DW}+}(\mathbf{k}_a,N+1)\rangle. \end{aligned} \tag{1}$$

In this amplitude the ion before and after excitation is supposed to be in the states $|\alpha_a,J_a,M_a\rangle$ and $|\alpha_b,J_b,M_b\rangle$ with a well-defined total angular momentum J,M and α denote all the additional quantum numbers as needed for a unique specification of the states. In the above expression, V_{in} is the interaction between incident electron and the ion. V_d is the distortion potential which is chosen to be the function of the position coordinate of the scattered electron only, i.e., r_{N+1}. In expression (1), $\phi_{a,b}$ represent N-electron target wave functions while $F_{a,b}^{\mathrm{DW}+(-)}$ denote the projectile electron distorted-wave functions which are calculated in the presence of distortion potential V_d. In this notation, the "+" sign refers to an outgoing wave, while the "−" sign denotes an incoming wave. $\mathcal{A}$ is the antisymmetrization operator that takes into account the exchange of the projectile electron with the target electrons. $\mu_{a,b}$ are the spin projections of electrons in the initial and final channel. $k_{a,b}$ are the relativistic wave numbers,

$$k_{a,b} = \frac{\sqrt{E_{a,b}(E_{a,b}+2c^2)}}{c}, \tag{2}$$

where $E_{a,b}$ are the relativistic energies (including the rest mass of the electron). The coordinate system is chosen in such a way that the incident electron defines the z axis, and the electrons are scattered in the xz plane with the scattering angle θ as the angle between the wave vectors $\mathbf{k}_a$ and $\mathbf{k}_b$ of the incident and scattered electron, respectively. In order to evaluate the amplitude (1) we need to know the explicit form of both, interaction operators and electronic wave functions. Therefore, in the following, we shall discuss these ingredients in more detail.

1. Interaction potential

The interaction between the (incident) electron and the target in Eq. (1),

$$\begin{aligned} V_{\mathrm{in}}(\mathbf{r}_i,\mathbf{r}_j) &= V^C(\mathbf{r}_i,\mathbf{r}_j)+V^B(\mathbf{r}_i,\mathbf{r}_j) \\ &= \sum_{i<j}\left(\frac{1}{r_{ij}}-\alpha_i\cdot\alpha_j\frac{1}{r_{ij}}+\frac{1}{2}(\alpha_i\cdot\boldsymbol{\nabla}_i)(\alpha_j\cdot\boldsymbol{\nabla}_j)r_{ij}\right), \end{aligned} \tag{3}$$

contains both the Coulomb repulsion V^C as well as the relativistic Breit interaction V^B (the second and third terms), which represent the contributions from the magnetic interaction between electrons and classical retardation due to finite propagation of the action. In the above expression, α_i are the Dirac matrices. The reduction of scattering amplitude in terms of angular coefficients and radial integrals for Coulomb interaction has already been discussed in our previous work [27]. In addition, we include the Breit interaction into the scattering amplitudes by following the paper by Grant and Pyper [28] to decompose the overall amplitude into products of radial integrals and angular coefficients.

2. Distortion potential

In order to obtain DWs, we compose the distortion potential as the sum of a direct part $V_{\mathrm{st}}(r)$ (or static potential) and an exchange part $V_{\mathrm{ex}}(r)$,

$$V_d(r) = V_{\mathrm{st}}(r)+V_{\mathrm{ex}}(r). \tag{4}$$

The first term $V_{\mathrm{st}}(r)$ is a spherically symmetric distorting potential which is obtained from the charge distribution of the atomic wave functions. This is a static atomic potential since the atomic wave functions are assumed not to be distorted by the projectile electron. In the present calculations we choose $V_{\mathrm{st}}(r)$ as the final excited-state potential of the ion with nuclear charge Z and number of electrons N,

$$\begin{aligned} V_{\mathrm{st}}(r) = -\frac{Z-N}{r}+\sum_{j\in\text{all subshells}}\mathcal{N}_j\int_0^\infty\big[P^2_{n_j\kappa_j}(r_j) \\ +Q^2_{n_j\kappa_j}(r_j)\big]\frac{1}{r_>}dr. \end{aligned} \tag{5}$$

Here $\mathcal{N}_j$ is the occupation number of the jth subshells and the electron in it is represented by quantum number $n_j\kappa_j$. P and Q are the larger and smaller components of the radial wave functions of ionic orbitals. These bound orbital wave functions are calculated by using the GRASP92 code of Parpia *et al.* [29].

In the present calculation we also include dynamic effects in the atomic potential such as electron exchange distortion. The exchange potential has also been derived from the static potential $V_{\rm st}$ by taking the commonly used local energy-dependent form [30]

$$V_{\rm ex}(r)=\frac{1}{2}\left[\left(\frac{1}{2}k^2-V_{\rm st}(r)+\frac{3}{10}[3\pi^2\rho(r)]^{\frac{2}{3}}\right)-\left\{\left(\frac{1}{2}k^2-V_{\rm st}(r)+\frac{3}{10}[3\pi^2\rho(r)]^{\frac{2}{3}}\right)^2+4\pi\rho(r)\right\}^{\frac{1}{2}}\right]. \quad (6)$$

Here $\rho(r)$ is the charge density which is given by

$$\rho(r)=\frac{1}{4\pi r^2}\sum_{j\in\text{all subshells}}\mathcal{N}_j\left[P^2_{n_j\kappa_j}(r_j)+Q^2_{n_j\kappa_j}(r_j)\right]. \quad (7)$$

3. *Continuum wave function*

The projectile electron DW functions $F^{\rm DW\pm}_{{\rm ch},\mu_{\rm ch}}$ are expanded into partial waves as

$$F^{\rm DW\pm}_{{\rm ch},\mu_{\rm ch}}(\mathbf{k}_{\rm ch},\mathbf{r})=\frac{1}{(2\pi)^{3/2}}\sum_{\kappa m}e^{\pm i\Delta_\kappa}a^{\mu_{\rm ch}}_{{\rm ch},\kappa m}(\hat{\mathbf{k}}_{\rm ch})\times\frac{1}{r}\begin{pmatrix}f_\kappa(r)\chi_{\kappa m}(\hat{\mathbf{r}})\\ ig_\kappa(r)\chi_{-\kappa m}(\hat{\mathbf{r}})\end{pmatrix}, \quad (8)$$

with

$$a^{\mu_{\rm ch}}_{{\rm ch},\kappa m}(\hat{\mathbf{k}}_{\rm ch})=4\pi i^l\left[\frac{E_{\rm ch}+c^2}{2E_{\rm ch}}\right]^{\frac{1}{2}}\times\sum_{m_l}(l\,m_l\,1/2\;\mu_{\rm ch}|j\,m)Y^*_{lm_l}(\hat{\mathbf{k}}_{\rm ch}). \quad (9)$$

We use "ch" to denote either the initial channel a or the final channel b. Δ_κ is the phase (Coulomb+scattering) shift. f_κ and g_κ are the large and small components of the radial wave functions and the $\chi_{\pm\kappa m}$ are the spinor spherical harmonics,

$$\chi_{\kappa m}(\hat{\mathbf{r}},\sigma)=\sum_{\mu\nu}\left(\ell\mu\frac{1}{2}\nu\middle|jm\right)Y_{\ell\mu}(\hat{\mathbf{r}})\psi_{\frac{1}{2}\nu}(\sigma), \quad (10)$$

$$\chi_{-\kappa m}(\hat{\mathbf{r}},\sigma)=\sum_{\mu\nu}\left(\tilde{\ell}\mu\frac{1}{2}\nu\middle|jm\right)Y_{\tilde{\ell}\mu}(\hat{\mathbf{r}})\psi_{\frac{1}{2}\nu}(\sigma). \quad (11)$$

Here j is the total angular momentum of the electron, m is the z component of j, $\tilde{\ell}=2j-\ell$, $(\ell_1m_1\ell_2m_2|\ell_3m_3)$ is a Clebsch-Gordan coefficient, the $Y_{\ell m}(\hat{\mathbf{r}})$ is the spherical harmonic, and $\psi_{\frac{1}{2}\nu}(\sigma)$ is a spinor basis function. κ is the relativistic angular quantum number, $\kappa=\pm(j+1/2)$ for $l=j\pm1/2$.

The large and small components f_κ and g_κ of the continuum wave functions satisfy the coupled Dirac equations,

$$\left(\frac{d}{dr}+\frac{k}{r}\right)f_\kappa(r)-\frac{1}{c}(c^2-V_d+E_{\rm ch})g_\kappa(r)=0, \quad (12)$$

$$\left(\frac{d}{dr}-\frac{k}{r}\right)g_\kappa(r)+\frac{1}{c}(-c^2-V_d+E_{\rm ch})f_\kappa(r)=0, \quad (13)$$

for the DW potential V_d as described above. These coupled equations can be solved numerically by accounting for the boundary conditions

$$f_\kappa(r)\overset{r\to\infty}{\longrightarrow}\frac{1}{k}\sin\left(k_{\rm ch}r-\frac{l\pi}{2}-\eta\ln 2k_{\rm ch}r+\Delta_\kappa\right), \quad (14)$$

$$g_\kappa(r)\overset{r\to\infty}{\longrightarrow}\frac{c}{c^2+E_{\rm ch}}\cos\left(k_{\rm ch}r-\frac{l\pi}{2}-\eta\ln 2k_{\rm ch}r+\Delta_\kappa\right), \quad (15)$$

where $\eta=Z/v$ is the Sommerfeld's parameter, with v being the velocity of the electron.

B. Scattering parameters

Having discussed all the ingredients of the scattering amplitude, we can use it to calculate other properties of the electron-ion collision process. For the given normalization of the amplitude, for instance, the differential cross section (DCS) is given by

$$\frac{d\sigma(\theta)}{d\omega}=\frac{1}{2(2J_a+1)}\sum_{\substack{M_a,\mu_a\\M_b,\mu_b}}|f(J_a,M_a,\mu_a;\;J_b,M_b,\mu_b,\theta)|^2, \quad (16)$$

where we need to sum over the (unobserved) spins of the incident and scattered electron as well as the magnetic substates of the target ion in its initial and final state. The integrated cross section (ICS) is obtained by integrating the DCS (16) over the all scattering angles. Similarly, after averaging only over initial magnetic sublevels M_a, one can easily obtain the cross section for excitation to a specific final magnetic sublevel M_b. In the present work we consider the excitation of an electron from the $ns_{1/2}$ to the $np_{1/2}$ and $np_{3/2}$ levels, which are both related to the ground state by electric-dipole transitions. However, only the $np_{3/2}$ levels can become aligned due to this excitation and can give rise to an anisotropic and polarized photon emission. Since in electron-photon coincidence experiments the photon is observed at 90° relative the electron beam, we can restrict ourselves to this angle. For 90°, the polarization of the emitted photons can be expressed in terms of magnetic sublevel cross sections as

$$P=\frac{3(\sigma_{1/2}-\sigma_{3/2})}{3\sigma_{3/2}+5\sigma_{1/2}}, \quad (17)$$

where $\sigma_{1/2}$ and $\sigma_{3/2}$ denote the cross sections for electron-impact excitation from the ground level $ns_{1/2}$ to the $M_b=1/2$ and $3/2$ magnetic sublevels of the $np_{3/2}$ level.

III. RESULTS AND DISCUSSION

We have performed relativistic distorted-wave (RDW) calculations for electron-impact resonance transitions $ns_{1/2}$-$np_{1/2}$ and $ns_{1/2}$-$np_{3/2}$ in singly ionized metal ions. Here $n=3$ for Mg^+ ([Ne]3s), $n=4$ for Ca^+ ([Ar]4s), $n=4$ for Zn^+ ([Ar]3d^{10}4s), $n=5$ for Cd^+ ([Kr]4d^{10}5s), and $n=6$ for Ba^+ ([Xe]6s). We have used the GRASP92 code [29] to obtain the wave functions for the ground and excited states as well as

TABLE I. Comparison of oscillator strength f_{osc} for the transitions $np_{1/2}$-$ns_{1/2}$ and $np_{3/2}$-$ns_{1/2}$ in various ions.

Ion	Transition	GRASP	Experiment	Other theories
Mg^+	$3p_{1/2}$-$3s_{1/2}$	0.312	–	0.302[b,c]
	$3p_{3/2}$-$3s_{1/2}$	0.632	0.64±0.03[a]	0.605[b,c]
Ca^+	$4p_{1/2}$-$4s_{1/2}$	0.364	–	0.330[c,d]
	$4p_{3/2}$-$4s_{1/2}$	0.735	0.66±0.02[a]	0.682[c,d]
Zn^+	$4p_{1/2}$-$4s_{1/2}$	0.251	0.249±0.050[e], 0.243[c]	0.317[e]
	$4p_{3/2}$-$4s_{1/2}$	0.550	0.467±0.093[e], 0.543[c]	0.642[e]
Cd^+	$5p_{1/2}$-$5s_{1/2}$	0.256	–	0.256[f], 0.230[c,g]
	$5p_{3/2}$-$5s_{1/2}$	0.560	–	0.548[f], 0.390[c,g]
Ba^+	$6p_{1/2}$-$6s_{1/2}$	0.416	0.348±0.090[c,h]	0.342[i]
	$6p_{3/2}$-$6s_{1/2}$	0.887	0.690±0.030[c,h]	0.742[i]

[a]Gallagher [32].
[b]MCHF calculations of Fischer *et al.* [33].
[c]NIST database [31].
[d]Fuhr and Wiese [34].
[e]Mayo *et al.* [35].
[f]HFR calculations of Xu *et al.* [36].
[g]Fuhr and Wiese [37].
[h]Davidson *et al.* [38].
[i]RMP calculations of Migdalek and Wyrozumska [39].

oscillator strengths f_{osc} of the resonance transitions of these ions. Table I. shows the comparison of our calculated oscillator strengths for the fine-structure transitions of all the ions with the experiment and recent theoretical calculations, along with the values recommended in the NIST database [31]. For the $3p_{3/2}$-$3s_{1/2}$ transition in Mg^+, our oscillator strength is in very good agreement with the measured value of Gallagher [32]. Also, for both the fine-structure transitions in Mg^+, our results are in reasonable agreement with the multiconfiguration Hartree-Fock (MCHF) calculations of Fischer *et al.* [33] and the same values recommended in the NIST database [31]. A similar comparison for Ca^+ shows that our oscillator strengths are slightly higher than the measurement of Gallagher [32], as well as theoretical oscillator strengths listed in the NIST database [31,34]. In case of Zn^+, our calculated oscillator strengths for $4p_{1/2}$-$4s_{1/2}$ and $4p_{3/2}$-$4s_{1/2}$ transitions are in good agreement with the recently reported experimental and multiconfigurational relativistic Hartree-Fock (MCHFR) calculations of Mayo *et al.* [35], as well as the experimental values from NIST database. For Cd^+, our calculated oscillator strengths are in good agreement with the pseudorelativistic Hartree-Fock (HFR) calculations of Xu *et al.* [36] but somewhat higher than the theoretical values of the NIST database [31,37]. Finally for Ba^+, our oscillator strengths are compared with the measurements of Refs. [31] and [38], as well as relativistic model potential (RMP) calculation [39]. For the $6p_{1/2}$-$6s_{1/2}$ transition our value lies within the experimental uncertainty, whereas our oscillator strength for the $6p_{3/2}$-$6s_{1/2}$ transition is slightly higher than the other results presented in Table I. However, as we will see later in Figs. 5(c) and 5(d), our cross sections for fine-structure transitions in Ba^+ still agree very well with the measurements of Crandall *et al.* [8].

Further, the results for DCS, ICS, and the degree of linear polarization of photon emission are obtained in the electron-energy range up to 300 eV for the resonance transitions. The calculations have been performed by taking into account the relativistic Breit corrections. Figures 1– 5 compare the results from our computations with the available measurements and other theoretical calculations. For further comparison, we have also performed semirelativistic DW calculations for the ICS by using the Los Alamos code [40]. However, this code helps to calculate only the ICS as summed over all the magnetic substates but not for the ICS for the sublevels or the DCS and any other scattering parameter. On the other hand, our RDW code has an advantage that it can calculate all possible differential and angle integrated scattering parameters, also in a fully relativistic manner. In the following, we summarize our results for the individual ions.

A. Mg^+

Figures 1(a)–1(d) present our RDW results for Mg^+. In the top row, we show the DCS at 35 eV (left-hand side) and at 50 eV (right-hand side). The bottom left-hand and bottom right-hand panels display ICS and polarization fraction, respectively.

We compare our DCS results with the available experimental data at 35 and 50 eV and with the five-state CC [14] and NRDW calculations [22]. As can be seen from the figure, we show these results for the fine-structure unresolved $3s$-$3p$ transition. This is because the RDW excitation cross section for $3s_{1/2}$-$3p_{1/2}$ is nearly half the cross sections for $3s_{1/2}$-$3p_{3/2}$, which suggests that the excited states in Mg^+ can be well described by LS coupling. Therefore, we take the sum of the two DCS for these fine-structure transitions and displayed in Figs. 1(a) and 1(b). The experimental data of Williams *et al.* [13,14] were normalized to the five-state CC calculations at $\theta = 12^\circ$. We did not renormalized this data with our calculations as CC results agree with our results at 12° as well. We see that all the three theoretical curves agree reasonably with the measurements, which are available in the limited small scattering angle range of 20°. This is not surprising as, being a dipole allowed transition, most calculations (even first Born) are expected to give reliable results near forward-scattering angles. For intermediate and large scattering angles, there are large deviations among the theoretical results and hence more experimental data are desired for this range of scattering angles in order to confirm or deny these structures. The present DCS calculations show a broad dip near 120° while the five-state CC calculations show a sharp dip slightly shifted to smaller scattering angles. The NRDW DCS results [22] tend to oscillate rapidly at larger angles, which may be due to nonconvergence of partial waves in these calculations.

Figure 1(c) shows the comparison of our ICS results for Mg^+ with the scaled cross sections of Kim [16] as well as semirelativistic DW calculations from the Los Alamos code [40]. All the three theoretical curves in Fig. 1(c) tend to merge as the incident electronenergy increases. However, near threshold excitation, the other two theocratical curves lie below our results. Until now, we have discussed results for an unresolved transition. Further, we show the polarization fraction for the $3p_{3/2}$-$3s_{1/2}$ line in Mg^+ as a function of electron energy [Fig. 1(d)]. There are no theoretical calculations or experimental data available for comparison. We see from

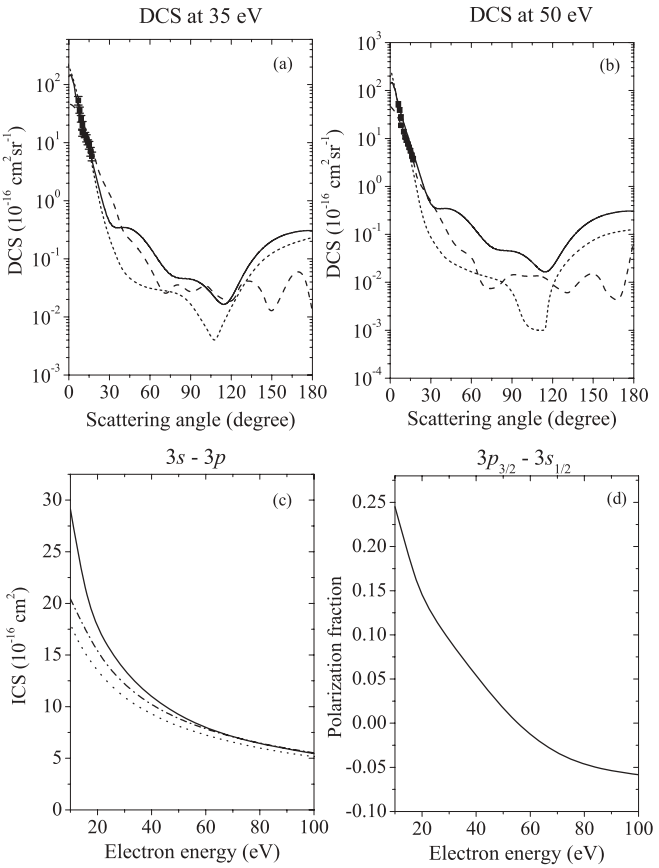

FIG. 1. Electron-impact excitation of Mg^+: (a) DCS at 35 eV; (b) DCS at 50 eV; (c) ICS for $3s$-$3p$ (d) polarization fraction for $3p_{3/2}$-$3s_{1/2}$. Solid curve, present RDW calculations; dashed curves, NRDW calculations [22]; short dashed curves, five-state CC calculations [14]; dotted curves, scaled results [16]; dashed-dotted curve, Los Alamos code [40]; experimental points with error bars, Williams *et al.* [13,14].

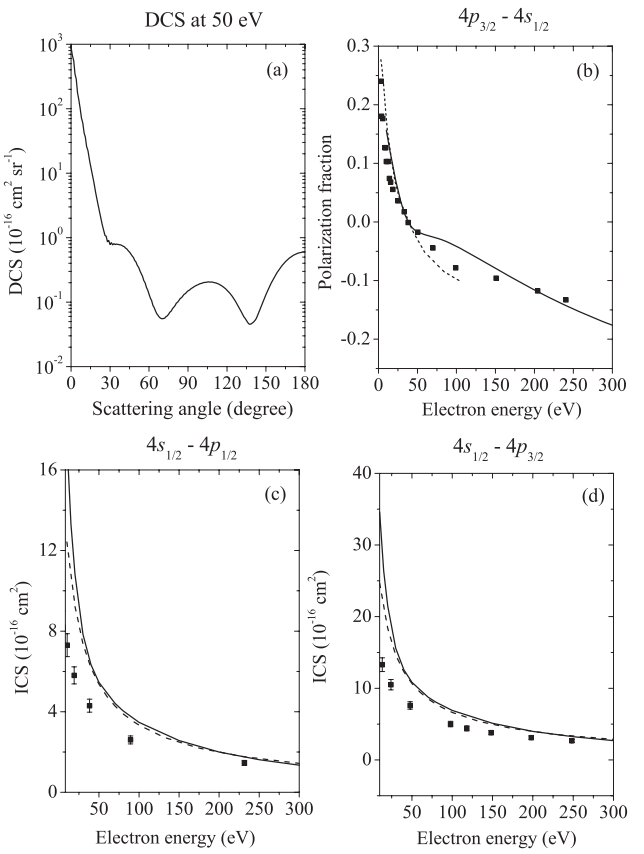

FIG. 2. Electron-impact excitation of Ca^+: (a) DCS at 50 eV; (b) polarization fraction for $4p_{3/2}$-$4s_{1/2}$; (c) ICS for $4s_{1/2}$-$4p_{1/2}$; (d) ICS for $4s_{1/2}$-$4p_{3/2}$. Solid curve, present RDW calculations; dashed curves, Los Alamos code [40]; short dashed curve, three-state CC calculations [19]; experimental points, Taylor and Dunn [9].

the Fig. 1(d) that our calculated polarization decreases as the energy of the incident electron increases and becomes negative above 50 eV. This is qualitatively in accord with one's expectations that at threshold the momentum transfer should be along the electron direction, and at high energy should be dominantly transverse to the electron direction of motion. Since the momentum transfer from the electron to target is connected to the alignment of the excited target, the polarization of the emitted radiation should be positive near threshold and starts getting negative at high energies.

B. Ca^+

In contrast to Mg^+ ions, the top left-hand figure shows DCS at one energy, i.e., at 50 eV while the top right-hand panel displays linear polarization. The ICSs for fine-structure transitions are shown in the bottom row.

There are no experimental or theoretical DCS data available for comparison, therefore, as an illustration we show in Fig. 2(a) the DCS for the $4s$-$4p$ resonance transition at 50 eV. Again we present results for an unresolved transition since LS coupling can be allowed for Ca^+. As compared to DCS for Mg^+, the forward peak of DCS for Ca^+ is approximately five times larger and the DCS curve shows two well-defined minima at $\theta = 70^\circ$ and 140°. We now turn to the fine-structure transition and display in Fig. 2(b) the polarization fraction for the K line ($4p_{3/2}$-$4s_{1/2}$) in Ca^+ as a function of electron energy. We compare our results with the measurements reported by Taylor and Dunn [9], as well as with the three-state CC calculations of Ref. [19]. The overall agreement of our results is reasonable with the experimental as well as theoretical results. However, at the intermediate energy range (50–150 eV), the measured polarization lies between the two calculations.

Taylor and Dunn [9] also measured absolute excitation cross sections for fine-structure resolved $4s_{1/2}$-$4p_{1/2}$ (H-line) and $4s_{1/2}$-$4p_{3/2}$ (K-line) transitions. Figures 2(c) and 2(d) display a comparison of our ICS results with these measurements, as well as with semirelativistic DW calculations from the Los Alamos code [40]. From these two figures we find that our results for both the fine-structure transitions agree well in shape with the experimental data while the agreement in magnitude improves as we go to higher energies. Also the calculations from the Los Alamos code [40] agree very well with our results for both transitions. It is important to mention that in contrast to the available nonrelativistic calculations, our RDW method

can deal with fine-structure resolved transitions explicitly and hence is more suitable for describing fine-structure transitions.

C. Zn^+

In Fig. 3 we present our results for excitation of Zn^+. Similar to Mg^+, the top row shows the DCS results and the bottom left-hand and right-hand figures exhibit the ICS and polarization fraction, respectively. As shown in Fig. 3(a), we compare our DCS results for $4s$-$4p$ transition at 50 eV with the theoretical results in multiple LS-term CC [21] and NRDW [22] approximations as well as the relative measurements of Williams *et al.* [13]. These experimental data were normalized to five-state CC calculations [14] at $\theta = 12^\circ$. Our results are in good agreement with the experimental values and the other two calculations in the small scattering angle range. Again the three theoretical DCS curves have different shapes over the large scattering angles, but these features could not be confirmed due to unavailability of measurements in this scattering angle range. Figure 3(b) shows a comparison of our present relativistic calculations at 75 eV with the experimental data and five-state CC calculations of Chutjian *et al.* [12], as well as the NRDW results [22]. Similar to the case observed at 50 eV, all three calculations are in good agreement with the experimental data near forward angles but differ at larger scattering angles. At both these energies a comparison of our results with experiment shows similar features as described in Fig. 1 for Mg^+.

Figure 3(c) displays our ICS results for the $4s$-$4p$ excitation in Zn^+ as compared with the scaling method of Kim [16] and DW calculations from the Los Alamos code [40]. Overall, our results and the calculations from the Los Alamos code [40] are in good agreement, but the scaled cross sections of Kim [16] are much lower in the entire energy range and do not seem to follow the same high-energy behavior. Figure 3(d) shows the comparison of our results of the polarization fraction for the fine-structure transition $4p_{3/2}$-$4s_{1/2}$ with the experimental data of Roger *et al.* [10]. To the best of our knowledge, there are no other theoretical results available for comparison. We see that our results agree reasonably with the measurements at large electron-impact energies and show the expected high-energy behavior.

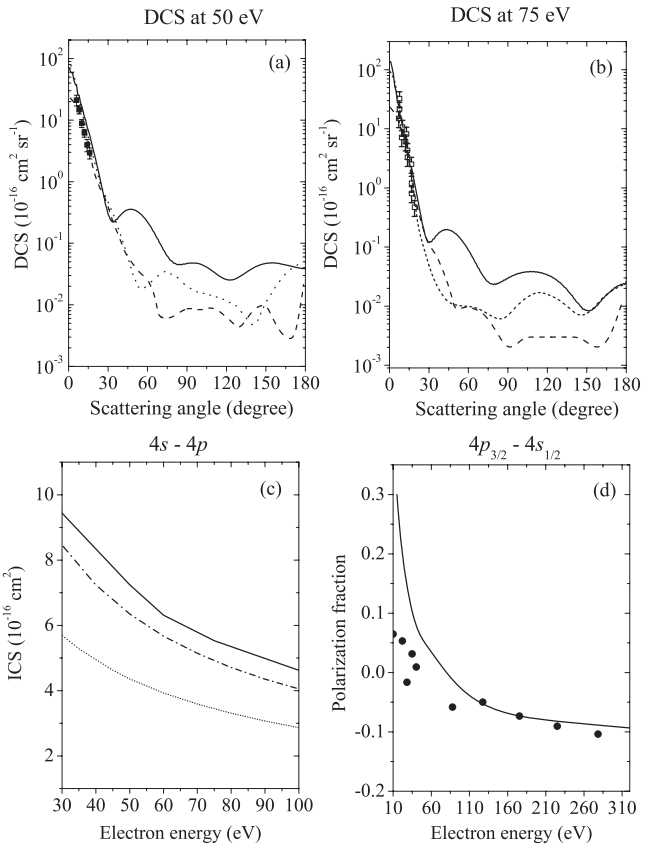

FIG. 3. Electron-impact excitation of Zn^+: (a) DCS at 50 eV; (b) DCS at 75 eV; (c) ICS for $3s$-$3p$; (d) polarization fraction for $3p_{3/2}$-$3s_{1/2}$. Solid curve, present RDW calculations; dashed curves, NRDW calculations [22]; dotted curve, CC calculations [21]; short dashed curve, five-state CC calculations [12]; short dotted curves, scaled results [16]; dashed-dotted curve, Los Alamos code [40]; squares with error bars, Williams *et al.* [13]; open squares with error bars, Chutjian *et al.* [12]; circles, Roger *et al.* [10].

D. Cd^+

Through Fig. 4 we have shown the results for Cd^+, similar to Mg^+ and Zn^+ in earlier figures. Figures 4(a) and 4(b) (top

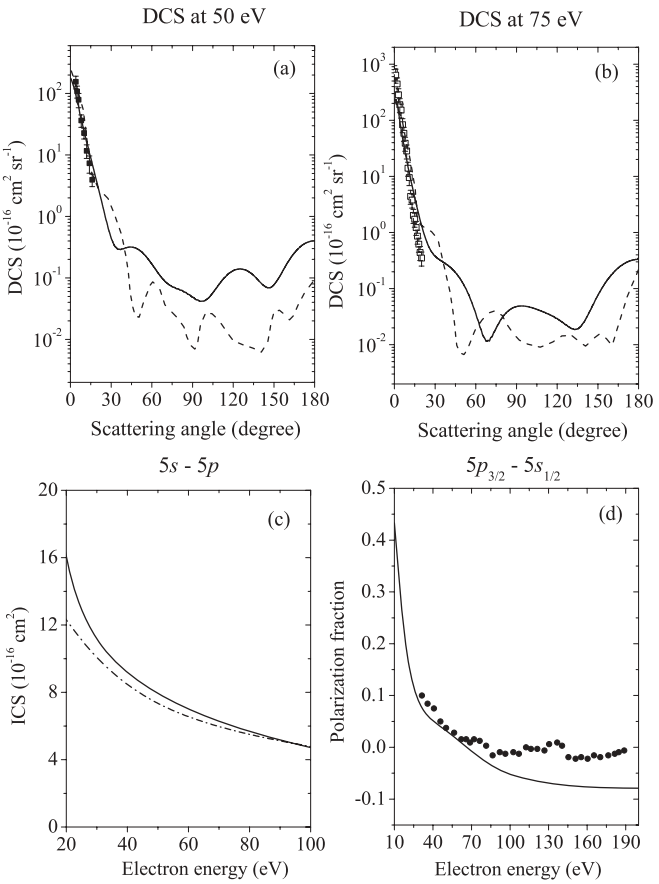

FIG. 4. Electron-impact excitation of Cd^+: (a) DCS at 50 eV; (b) DCS at 75 eV; (c) ICS for $5s$-$5p$; (d) polarization fraction for $5p_{3/2}$-$5s_{1/2}$. Solid curve, present RDW calculations; dashed curves, NRDW calculations [22]; dashed-dotted curve, Los Alamos code [40]; squares with error bars, Williams *et al.* [13]; open squares with error bars, Chutjian [41]; circles, Goto *et al.* [42].

panel) show our DCS results for the $5s$-$5p$ transition in Cd^+ at 50 and 75 eV, respectively. Here we compare our DCS results with the NRDW calculations [22] and experimental data of Williams *et al.* [13] at 50 eV and Chutjian [41] at 75 eV. The behavior of the present DCS results for Cd^+ is similar to the features as discussed earlier for Mg^+ and Zn^+. Our results are in good agreement with the measurements as well as other theoretical results in the forward-scattering angle region. Again the fast oscillations in the NRDW results [22] show that these results may not have been converged. In Fig. 4(c) (bottom left-hand panel) we compare our ICS for the $5s$-$5p$ transition in Cd^+ with DW calculations from the Los Alamos code [40]. Both the calculations merge together as the electron energy increases. Similar to the previous comparisons, Fig. 4(d) (bottom right-hand panel) displays the polarization fraction as a function of electron energy for the $5p_{3/2}$-$5s_{1/2}$ transition. In this figure we compare our results with the measurements of Goto *et al.* [42]. Above 70 eV, our calculations show negative values similar to the experimental values of polarization fraction, but the experimental data lie higher than our results.

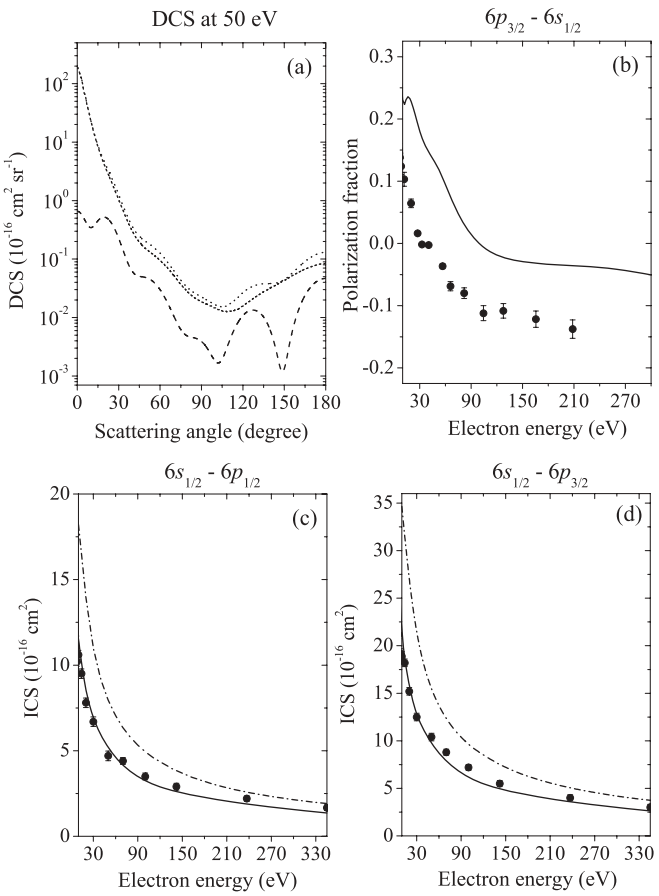

FIG. 5. Electron-impact excitation of Ba^+: (a) DCS at 50 eV; (b) polarization fraction for $6p_{3/2}$-$6s_{1/2}$; (c) ICS for $6s_{1/2}$-$6p_{1/2}$; (d) ICS for $6s_{1/2}$-$6p_{3/2}$. Solid curve, present RDW calculations; dashed curves, present RDW DCS for $6s_{1/2}$-$6p_{1/2}$; short dashed curve, present RDW DCS for $6s_{1/2}$-$6p_{3/2}$; dotted curve summed DCS for $6s$-$6p$; dashed-dotted curve, Los Alamos code [40]; circles with error bars, Crandall *et al.* [8].

E. Ba^+

Finally, in Fig. 5 we present our results for Ba^+ ions. Similar to Ca^+ ions, to the best of our knowledge, there are no other experimental or theoretical DCS results available for comparison. Therefore, Fig. 5(a) (top left-hand panel) shows our DCS results for the fine-structure resolved as well as the unresolved $6s$-$6p$ transition in Ba^+ only at one energy, i.e., 50 eV. Since Ba^+ can be said to be a relatively heavier ion, we see that the relativistic effects play a significant role. Consequently, the ratio of DCS for $6s_{1/2}$-$6p_{3/2}$ and $6s_{1/2}$-$6p_{1/2}$ excitations is not nearly 2 for Ba^+, as was seen earlier for other ions, in particular, for Mg^+ and Ca^+. Moreover, unlike the other four ions discussed earlier, the individual DCSs for these two fine-structure transitions in Ba^+ have a very different shape [Fig. 5(a)]. At 50 eV we observe that the summed DCS for unresolved transition is dominated by the DCS for the $6s_{1/2}$-$6p_{3/2}$ excitation. The polarization fraction for the $6p_{3/2}$-$6p_{1/2}$ transition is shown in Fig. 5(b) (top right-hand panel), where we compare our results with the measurements of Crandall *et al.* [8]. Our calculations are seen to overestimate the polarization measurements over the entire electron-energy range. The source of this discrepancy could be due to the cascade effect in the experimental data. Crandall *et al.* [8] also measured the absolute cross sections for $6s_{1/2}$-$6p_{1/2}$ and $6s_{1/2}$-$6p_{3/2}$ transitions. Figures 5(c) and 5(d) (bottom panel) show the comparison of our ICS results with their experimental results. Our cross sections are in very good agreement with the measurements. We have also shown the results from semirelativistic DW Los Alamos code [40]. The comparison of our results with the results from the Los Alamos code and measurements shows that relativistic effects play an important role for Ba^+ and must be included in the theoretical model to interpret experimental data.

F. Analytic fits to cross sections

Since the transitions $ns_{1/2}$-$np_{1/2}$ and $ns_{1/2}$-$np_{3/2}$ are resonance transitions, their ICS takes on the Bethe-Born form at higher projectile electron energies, viz.,

$$\mathrm{ICS} = \frac{4\pi f_{\mathrm{osc}}}{E\triangle E}[b + \ln(E)]a_0^2. \tag{18}$$

In the above expression, E is the incident electron energy, $\triangle E$ is the excitation energy of the transition, a_0 is the Bohr radius, and b is the fitting constant. All energies are in Rydbergs. The oscillator strength f_{osc} is taken to be the same as given in Table I. We have fitted our cross sections to the above formula and the fitting constant b for all the transitions is given in

TABLE II. Values for the constant b from Eq. (18) for the resonance transition $ns_{1/2}$-$np_{1/2}$ and $ns_{1/2}$-$np_{3/2}$ in various ions.

Transition Ion	$ns_{1/2}$-$np_{1/2}$ b	$ns_{1/2}$-$np_{3/2}$ b
Mg^+	1.815	1.926
Ca^+	2.578	2.551
Zn^+	2.902	2.501
Cd^+	2.957	2.622
Ba^+	0.910	0.841

Table II. Our fitting is valid for impact energies above 30 eV and has an accuracy of 5%.

IV. CONCLUSIONS

In the present work we have extended the RDW method to study electron-impact excitation of singly charged metal ions with one electron in the outer shell, viz., Mg^+, Ca^+, Zn^+, Cd^+, and Ba^+. We calculated and presented differential and integrated cross sections as well as the polarization parameter for fine-structure resolved resonance transitions $ns_{1/2}$-$np_{1/2}$ and $np_{3/2}$ in these ions.

For DCS, our RDW calculations show very good agreement with the experimental data, along with other theoretical results in the near forward-scattering angle region where the measurements existed. However, for larger scattering angles all the theoretical curves have shown different structures which could not be confirmed owing to the unavailability of experimental data in this range. Further experiments are desirable to test the theories. We noticed that a large number of oscillations in the DCS from NRDW theory [22] seem to be due to nonconvergence of the partial waves.

We reported ICS for fine-structure transitions in Ca^+ and Ba^+ for which experimental data were available and, to the best of our knowledge, no other theoretical calculations have been reported for comparison. Our RDW calculations for these two ions have shown good agreement with the measurements. For rest of the ions, we showed ICS results for a fine-structure unresolved transition ns-np and found reasonable agreement with the other theoretical results. We have also provided the fitting to the ICS for their applications in plasma modeling.

We also presented linear polarization of the photon emission following the decay of the excited $np_{3/2}$ state to the ground $ns_{1/2}$ state. Our results are in good agreement with the available measurements and theoretical calculations for all the metal ions except for Ba^+. The reason for this discrepancy could be cascade effects which we neglected in the present calculations.

In the present calculations, to account full relativistic effects of the electron-electron interaction, we added the Breit interaction as a correction to the Coulomb interaction in first-order perturbation theory. Although inclusion of the Breit interaction did not have a very significant effect on the results presented in this paper, this has been expected to be of great importance for studying highly charged ions. As a further application of our present RDW method, we plan in the near future to apply it to study the electron-impact excitation of highly charged ions in the light of ongoing measurements.

ACKNOWLEDGMENTS

L.S. and A.S. acknowledge support from the Helmholtz Gemeinschaft and GSI (Nachwuchsgruppe VH-NG-421). R.S. acknowledges research grants in support of this work from the Council of Scientific and Industrial Research (CSIR), New Delhi, and IAEA, Vienna. S.F. acknowledges support by the FiDiPro programme of the Finnish Academy.

[1] L. Sharma, R. Srivastava, and A. D. Stauffer, Phys. Rev. A **78**, 014701 (2008).
[2] R. K. Gangwar, L. Sharma, R. Srivastava, and A. D. Stauffer, Phys. Rev. A **81**, 052707 (2010).
[3] R. K. Chauhan, R. Srivastava, and A. D. Stauffer, J. Phys. B **38**, 2385 (2005).
[4] D. V. Fursa, C. J. Bostock, and I. Bray, Phys. Rev. A **80**, 022717 (2009).
[5] O. Zatsarinny and K. Bartschat, Phys. Rev. A **79**, 042713 (2009).
[6] D. H. Sampson, H. L. Zhang, and C. J. Fontes, Phys. Rep. **477**, 111 (2009).
[7] C. J. Bostock, D. V. Fursa, and I. Bray, Phys. Rev. A **80**, 052708 (2009).
[8] D. H. Crandall, P. O. Taylor, and G. H. Dunn, Phys. Rev. A **10**, 141 (1974).
[9] P. O. Taylor and G. H. Dunn, Phys. Rev. A **8**, 2304 (1973).
[10] W. T. Rogers, G. H. Dunn, J. O. Olsen, M. Reading, and G. Stefani, Phys. Rev. A **25**, 681 (1982).
[11] A. Chutjian and W. R. Newell, Phys. Rev. A **26**, 2271 (1982).
[12] A. Chutjian, A. Z. Msezane, and R. J. W. Henry, Phys. Rev. Lett. **50**, 1357 (1983).
[13] I. D. Williams, A. Chutjian, and R. J. Mawhorter, J. Phys. B **19**, 2189 (1986).
[14] I. D. Williams, A. Chutjian, A. Z. Msezane, and R. J. W. Henry, Astrophys. J. **299**, 1063 (1985).
[15] S. J. Smith, A. Chutjian, J. Mitroy, S. S. Tayal, R. J. W. Henry, K-F. Man, R. J. Mawhorter, and I. D. Williams, Phys. Rev. A **48**, 292 (1993).
[16] Y. K. Kim, Phys. Rev. A **65**, 022705 (2002).
[17] O. Zatsarinny and L. Bandurina, J. Phys. B **32**, 4793 (1999).
[18] J. V. Kennedy, V. P. Myerscough, and M. R. C. McDowell, J. Phys. B **11**, 1303 (1978).
[19] P. G. Burke and D. L. Moores, J. Phys. B **1**, 575 (1968).
[20] J. Mitroy, D. C. Griffin, D. W. Norcross, and M. S. Pindzola, Phys. Rev. A **38**, 3339 (1988).
[21] M. S. Pindzola, N. R. Badnell, R. J. W. Henry, D. C. Griffin, and W. L. van Wyngaarden, Phys. Rev. A **44**, 5628 (1991).
[22] A. W. Pangantiwar and R. Srivastava, J. Phys. B **21**, L219 (1988).
[23] L. Sharma, R. Srivastava, and A. D. Stauffer, J. Phys. B **40**, 3025 (2007).
[24] G. Auendorf, F. Jüttemann, K. Muktavat, L. Sharma, R. Srivastava, A. D. Stauffer, K. Bartschat, D. V. Fursa, I. Bray, and G. F. Hanne, J. Phys. B **39**, 2403 (2006).
[25] F. Jüttemann, G. F. Hanne, O. Zatsarinny, K. Bartschat, R. Srivastava, R. K. Gangwar, and A. D. Stauffer, Phys. Rev. A **81**, 012705 (2010).
[26] Lalita Sharma, R. Srivastava, and A. D. Stauffer, Phys. Rev. A **76**, 024701 (2007).
[27] L. Sharma, Ph.D. thesis, IIT Roorkee, 2008.
[28] I. P. Grant and N. C. Pyper, J. Phys. B **9**, 761 (1976).
[29] F. A. Parpia, C. F. Fischer, and I. P. Grant, Comput. Phys. Commun. **94**, 249 (1996).
[30] F. A. Gianturco and S. Scialla, J. Phys. B **20**, 3171 (1987).
[31] [http://www.nist.gov/pml/data/asd.cfm].
[32] A. Gallagher, Phys. Rev. **157**, 24 (1967).

[33] C. F. Fischer, G. Tachiev, and A. Irimia, At. Data Nucl. Data Tables **92**, 607 (2006).
[34] J. R. Fuhr and W. L. Wiese, in *CRC Handbook of Chemistry and Physics*, 79th ed., edited by D. R. Lide (CRC Press, Boca Raton, FL, 1998), pp. 10-88–10-146.
[35] R. Mayo, M. Ortiz, and J. Campos, Eur. Phys. J. D **37**, 181 (2006).
[36] H. L. Xu, A. Persson, S. Svanberg, K. Blagoev, G. Malcheva, V. Pentchev, E. Biémont, J. Campos, M. Ortiz, and R. Mayo, Phys. Rev. A **70**, 042508 (2004).
[37] J. R. Fuhr and W. L. Wiese, in *CRC Handbook of Chemistry and Physics*, 86th ed., edited by D. R. Lide (CRC Press, Boca Raton, FL, 2005), pp. 10-93–10-155.
[38] M. D. Davidson, L. C. Snoek, H. Volten, and A. Dönszelmann, Astron. Astrophys. **255**, 457 (1992).
[39] J. Migdalek and M. Wyrozumska, J. Quant. Spectrosc. Radiat. Transfer **37**, 581 (1987).
[40] [http://aphysics2.lanl.gov/cgi-bin/ION/runlanl08d.pl].
[41] A. Chutjian, Phys. Rev. A **29**, 64 (1984).
[42] K. Hane, T. Goto, and S. Hattori, Phys. Rev. A **27**, 124 (1983).